Comprehensive γ-ray spectroscopy of rotational bands in the $N = Z + 1$ nucleus ^{61}Zn

L.-L. Andersson,[1] I. Ragnarsson,[2] D. Rudolph,[1] E. K. Johansson,[1] D. A. Torres,[3,*] C. Andreoiu,[1,†] M. P. Carpenter,[4] R. J. Charity,[5] C. J. Chiara,[5,‡] J. Ekman,[1,§] C. Fahlander,[1] C. Hoel,[5] O. L. Pechenaya,[6,‖] W. Reviol,[5] R. du Rietz,[1,¶] D. G. Sarantites,[5] D. Seweryniak,[4] L. G. Sobotka,[5] and S. Zhu[4]

[1]*Department of Physics, Lund University, S-22100 Lund, Sweden*
[2]*Department of Mathematical Physics, Lund Institute of Technology, S-22100 Lund, Sweden*
[3]*Departamento de Física, Universidad Nacional de Colombia, Bogotá, Colombia*
[4]*Physics Division, Argonne National Laboratory, Argonne, Illinois 60439, USA*
[5]*Chemistry Department, Washington University, St. Louis, Missouri 63130, USA*
[6]*Physics Department, Washington University, St. Louis, Missouri 63130, USA*

(Received 20 October 2008; published 18 February 2009)

The $^{61}_{30}$Zn$_{31}$ nucleus has been studied via the combined data of two fusion-evaporation reaction experiments using a ^{36}Ar beam and a ^{28}Si target foil. The experimental setups involved the Ge array GAMMASPHERE and neutron and charged particle detectors placed around the target position. The resulting level scheme comprises about 120 excited states connected via some 180 γ-ray transitions. In total, seven rotational structures were identified up to $I \sim 25$ or higher and compared with predictions from cranked Nilsson-Strutinsky calculations.

DOI: 10.1103/PhysRevC.79.024312 PACS number(s): 21.60.Cs, 23.20.En, 23.20.Lv, 27.50.+e

I. INTRODUCTION

Neutron-deficient nuclei in the mass $A \sim 60$ region are embraced by the high-j $1f_{7/2}$ and $1g_{9/2}$ orbitals. Holes and particles in these orbitals are known to characterize the high-spin states and, in particular, the features of collective rotational structures in the vicinity of doubly magic ^{56}Ni [1–7]. For example, a direct relation between the quadrupole deformation and the number of holes in the $1f_{7/2}$ orbital and particles in the $1g_{9/2}$ orbital has been empirically derived by Andreoiu *et al.* [1]. The spherical subshells placed in between, namely, $2p_{3/2}$, $1f_{5/2}$, and $2p_{1/2}$, are considered of low-j character, and they are thus less important when forming high-spin states in this region.

Starting at normal deformation (ND) with a few particles in the upper fp shell outside the soft doubly magic $N = Z = 28$ ^{56}Ni core, ^{61}Zn, like the other nuclei in the region, becomes well deformed and eventually superdeformed (SD), when the number of holes in the $1f_{7/2}$ orbital and particles in the $1g_{9/2}$ orbital rapidly increase with spin and excitation energy. Superdeformed bands are here defined as those with at least some four particle-holes in the $1f_{7/2}$ and four particles in the $1g_{9/2}$ orbital. In fact, a superdeformed band in ^{61}Zn has been reported by Yu *et al.* [5].

In the present paper, a high-spin study of ^{61}Zn is presented with firmer spin-parity assignments than in previously published papers. In Refs. [8–11], excited states were observed up to $I^\pi = 31/2^-$ at excitation energies just above 10 MeV, which can be reasonably well described within the framework of spherical shell-model calculations [11]. Another facet of especially superdeformed bands in a series of $N \sim Z$ nuclei is the possibility of probing isospin-dependent features in the second potential well, namely, the persistence or (re)occurrence of isoscalar neutron-proton pairing at high angular momenta. With the example of the presumed yrast superdeformed bands in ^{60}Zn and ^{61}Zn, this has been done in depth in Ref. [5]. However, our comprehensive analyses of normally deformed low-spin states in ^{61}Zn [11,12] revealed that the decay-out scheme and/or the tentative spin-parity assignment to the known superdeformed band in ^{61}Zn are in doubt, hence potentially seriously affecting the conclusions drawn in Ref. [5]. This conflicting situation has been resolved in the present paper, resulting in corrections to the experimental level scheme but leaving the theoretical interpretation regarding the superdeformed band (here denoted SD1) [5] in essence unchanged.

Based on significantly increased statistics, the experimentally observed energy levels of the present study involve six structures in the low-spin region, ND1–ND6, and seven high-spin structures, ND7–ND10 and SD1–SD3, in ^{61}Zn. The experimental details and setups in the two utilized experiments are described in Sec. II. The analysis and results are reported in Sec. III, which describes each structure separately and motivates its spin-parity assignment. In Sec. IV a comparison with predictions using cranked Nilsson-Strutinsky (CNS) calculations is made. The deformed shell-model calculations are first introduced, and the classification of the observed structures is discussed in detail.

II. EXPERIMENTAL DETAILS

The results presented in this paper originate from the combined statistics from two different experiments carried out using the GAMMASPHERE Ge-detector array [13] at Argonne National Laboratory. For a thorough description of

---

*Present address: University of the West of Scotland, High Street, Paisley, PA1 2BE Scotland, UK.
†Present address: Chemistry Department, Simon Fraser University, Burnaby, BC, V5A 1S6, Canada.
‡Present address: Nuclear Engineering Division, Argonne National Laboratory, Argonne, Illinois 60439, USA.
§Present address: Malmö högskola, S-20506 Malmö, Sweden.
‖Present address: Department of Radiation Oncology, Washington University School of Medicine, St. Louis, Missouri 63130, USA.
¶Present address: Department of Nuclear Physics, Australian National University, Canberra ACT 0200, Australia.

the experimental details, see Ref. [14]. A brief summary is given below.

In both experiments, the residues were formed via the fusion-evaporation reaction ^{36}Ar(^{28}Si, $2p1n$)^{61}Zn. The beam energies of 142 and 148 MeV allowed the produced ^{61}Zn nuclei to be formed at excitation energies up to some 30 MeV and angular momenta up to around $30\hbar$.

The present analysis groups the Ge detectors in GAMMASPHERE into so-called pseudorings due to their angular positions relative to the beam axis. For details, see Ref. [15]. These pseudorings are placed and labeled according to 30°, 53°, 70°, and 83°. Using the ratio between yields from the rings at 30° and 83° provides a figure sensitive to the multipolarity of the γ ray. The method and results are presented in Sec. III.

The evaporated neutrons are detected in a number of liquid scintillators placed around the target position in the forward direction [16]. Similarly, a combination of some elements in Microball [17] and a number of ΔE-E silicon strip telescopes were used to detect the charged particles emitted at the target position. Details about these detection systems can be found in Refs. [2,18].

III. ANALYSIS AND RESULTS

A kinematic correction [19,20] was used to improve the ordinary Doppler correction. The detected energy and angle of emission of the evaporated particles, as well as the type of particle, are utilized to reconstruct the recoil vector of the residual nuclei on an event-by-event basis. This improves the full width at half maximum (FWHM) of the emitted γ rays significantly [21]. However, above some 8 MeV excitation energy, the ^{61}Zn nuclei often emit the γ rays while still moving inside the target, resulting in a larger FWHM than for the γ rays deexciting the low-spin states. This is caused by the nucleus moving at a different speed inside the target than when it has left it. In total, the combined statistics from the two experiments result in a systematic uncertainty of about 1 keV per 1 MeV γ-ray energy for excitation energies above some 8 MeV.

The selection of nuclei of interest was done via the detected particles in the experimental setup and the identified type of particle in the software analysis. Here, always two protons and one neutron were demanded, corresponding to ^{61}Zn which represents the $2p1n$ evaporation channel. To account for the fact that neither the detection nor identification is 100% efficient, a so-called total-energy (TE) gate [22] can be used in the analysis. This gate will reduce the amount of contaminants in the spectra, as it utilizes the fact that the total energy of the γ rays and emitted particles should essentially be constant for all events. This means that if one or more particles in an event escape detection, the TE gate will exclude γ-ray transitions from such an event in the spectra of interest.

The analysis of ^{61}Zn utilized a so-called $\gamma\gamma\gamma$-cube created with E_γ-E_γ-E_γ coincidences using the RADWARE analysis package [23]. The triple coincidences naturally result in a very clean analysis but require a large amount of statistics. To confirm low-intensity transitions, the analysis was combined with E_γ-E_γ matrices. They reveal a larger amount of statistics, but they generally comprise a higher background level due to doublets or some remaining contaminations from other reaction channels. For the spectrum analysis, the code TV developed at the University of Cologne [24] was used.

For the low-spin states, the spin-parity assignments of the energy levels are adopted from Ref. [11]. For the high-spin structures, intensity ratios of γ rays observed in different detector rings in the setup are used to determine the multipolarities of the detected γ rays. This in turn provides the spin-parity assignments of the energy levels in the present level scheme. In the current analysis, the intensity ratio $R_{30-83} = Y(30°)/Y(83°)$ is used. Ratios for known stretched $\Delta I = 2$ reference transitions amount to $R_{30-83} \sim 1.6$–1.7, while stretched dipole transitions have $R_{30-83} \sim 0.7$–0.8.

The resulting level scheme of ^{61}Zn is shown in Fig. 1. Here, both the low-spin and high-spin parts are illustrated, and each structure is labeled according to their short-hand notation, ND1–ND10 and SD1–SD3. In addition, some structures consist of two bands, which are considered signature partners. In these cases, the band with positive signature is denoted A, and the band with negative signature, B.

Table I lists the energies of the excited levels with the connecting γ-ray transitions, their relative intensities, intensity ratios, and final multipolarity assignments. The intensities are given relative to the 124 keV ground-state transition. Furthermore, the resulting spin-parity assignments of the initial and final energy levels between which the transition takes place are listed. The table contains only the high-spin levels, and each structure is dealt with separately. During the analysis of the present data, a number of high-energy γ-ray transitions were observed but unlinked to any of the observed high-spin structures. These transitions are also included at the very end of Table I. Clearly, more statistics are necessary for these low-intensity transitions to be properly connected.

A. Structure SD1

Structure SD1 is the only high-spin structure in the current analysis that has been previously published [5]. In that publication, two γ-ray transitions connected the SD structure to the low-spin level scheme. These were the 5170 and the 5278 keV transitions. In Ref. [11], the spin-parity assignments in the low-spin part of the level scheme were fixed, revealing that the tentative spin assignments of structure SD1 from Ref. [5] were not possible any longer, based on the suggested decay-out pattern. However, the current analysis indicates that the decay-out pattern of Ref. [5] has to be modified as well. This conclusion is drawn from the $\gamma\gamma\gamma$-cube analysis combined with the multipolarity assignments of the other linking γ-ray transitions in the decay out of the structure. The present observations indicate that the 5170 and 5278 keV transitions both decay into the 6091 keV, $21/2^+$ energy level. As a result of the modified decay out in the current analysis and the firm spin assignments from Ref. [11], the 11368 keV energy level in structure SD1 has now been assigned $I^\pi = 25/2^+$, which agrees with the tentative assignments from Yu *et al.* [5].

The relative intensity of SD1 is around 5% of the 124 keV ground-state transition. The structure is connected to the low-spin part of the level scheme via a total of six γ-ray transitions. None of the connecting transitions are very strong,

TABLE I. Summary of the experimental results on high-spin states and γ rays associated with the deformed bands in ^{61}Zn. For details on the low-lying states and their decay scheme, see Refs. [11,12]. Intensities in this table are given relative to the ground-state transition of 124 keV, which is given an intensity of 100 units.

E_x (keV)	E_γ (keV)	I_{rel} (%)	R_{30-83}	Multipolarity	J_i^π ($\hbar$)	J_f^π ($\hbar$)
SD1						
29171(7)	3129(3)	0.4(2)	1.39(36)	$E2$	$57/2^+$	$53/2^+$
26042(6)	2820(3)	1.7(3)	1.50(19)	$E2$	$53/2^+$	$49/2^+$
23222(5)	2548(3)	3.8(4)	1.24(11)	$E2$	$49/2^+$	$45/2^+$
20674(4)	2311(2)	4.3(5)	1.56(13)	$E2$	$45/2^+$	$41/2^+$
18363(4)	2083(2)	5.3(5)	1.76(14)	$E2$	$41/2^+$	$37/2^+$
16280(3)	1849(2)	5.5(5)	1.68(13)	$E2$	$37/2^+$	$33/2^+$
14431(2)	1629(2)	4.7(8)	1.35(11)	$E2$	$33/2^+$	$29/2^+$
	1702(2)	0.5(3)		$(E1)$[a]	$33/2^+$	$33/2^{(-)}$
	2199(2)	0.4(2)		$E2$[a]	$33/2^+$	$29/2^+$
12802(2)	1434(1)	1.7(5)	1.45(18)	$E2$	$29/2^+$	$25/2^+$
	1542(2)	0.5(3)	1.44(16)[b]	$E2$[a]	$29/2^+$	$25/2^+$
	4305(5)	0.9(2)	1.38(27)	$E2$	$29/2^+$	$25/2^+$
	5314(5)	0.4(2)	1.32(23)	$E2$	$29/2^+$	$25/2^+$
12729(2)	2571(2)	3.3(4)	0.59(8)	$(E2/M1)$	$33/2^{(-)}$	$31/2^-$
12232(3)	4745(5)	0.9(3)		$E2$[a]	$29/2^+$	$25/2^+$
11368(2)	5278(5)	1.2(3)	1.32(23)[b]	$E2$	$25/2^+$	$21/2^+$
11260(3)	5170(4)	0.7(2)		$E2$[a]	$25/2^+$	$21/2^+$
8497(1)	868(1)	0.8(2)		$E1$[a]	$25/2^+$	$23/2^-$
	1198(2)	1.5(4)		$E2/M1$[a]	$25/2^+$	$23/2^+$
SD2A						
25451(7)	3052(4)	0.6(3)		$(E2)$[c]	$(53/2^-)$	$(49/2^-)$
22399(6)	2707(3)	2.1(4)		$E2$[c]	$(49/2^-)$	$(45/2^-)$
19692(5)	2380(2)	3.7(4)		$E2$[c]	$(45/2^-)$	$(41/2^-)$
17312(5)	1080(1)	0.7(5)		$E2/M1$[a]	$(41/2^-)$	$(39/2^-)$
	2104(2)	5.1(6)	1.28(16)	$E2$	$(41/2^-)$	$(37/2^-)$
15208(5)	1942(2)	3.0(6)	1.30(21)	$E2$	$(37/2^-)$	$(33/2^-)$
13266(4)	1736(2)			$(E2)$[c]	$(33/2^-)$	$(29/2^-)$
	3109(4)	0.6(3)	0.95(50)	$(M1)$	$(33/2^-)$	$31/2^-$
SD2B						
27086(8)	3228(4)	0.3(1)		$E2$[c]	$(55/2^-)$	$(51/2^-)$
23858(7)	2857(3)	1.1(4)		$E2$[c]	$(51/2^-)$	$(47/2^-)$
21001(6)	2528(3)	2.9(4)		$E2$[c]	$(47/2^-)$	$(43/2^-)$
18473(5)	2241(2)	3.8(7)		$E2$[c]	$(43/2^-)$	$(39/2^-)$
16232(5)	755(1)	0.9(3)		$E2/M1$[c]	$(39/2^-)$	$(37/2^-)$
	1024(1)	1.2(2)		$E2/M1$[c]	$(39/2^-)$	$(37/2^-)$
	2086(2)	1.8(3)	1.25(41)	$(E2)$	$(39/2^-)$	$(35/2^-)$
	2169(3)	0.8(2)	1.23(41)	$(E2)$	$(39/2^-)$	$(35/2^-)$
SD2C						
25282(8)	3041(4)	0.3(1)		$(E2)$[c]	$(53/2^-)$	$(49/2^-)$
22241(6)	2586(3)	1.0(3)		$(E2)$[c]	$(49/2^-)$	$(45/2^-)$
19655(6)	2198(2)	2.4(4)	1.36(23)	$E2$	$(45/2^-)$	$(41/2^-)$
17457(5)	1980(2)	2.9(4)	1.35(25)	$E2$	$(41/2^-)$	$(37/2^-)$
15477(5)	1811(2)	3.2(5)		$E2$[c]	$(37/2^-)$	$(33/2^-)$
13666(5)	1622(2)	3.1(5)		$E2$[c]	$(33/2^-)$	$(29/2^-)$
ND7						
26696(7)	3731(4)	0.6(2)		$(E2)$[c]	$(53/2^+)$	$(49/2^+)$
22965(6)	2905(3)	3.0(4)	1.37(17)	$E2$	$(49/2^+)$	$(45/2^+)$
20060(5)	2450(3)	3.8(4)	1.21(12)	$E2$[c]	$(45/2^+)$	$(41/2^+)$
17610(5)	2045(2)	4.3(5)	1.75(15)	$E2$	$(41/2^+)$	$(37/2^+)$
15565(4)	1683(2)	4.0(5)	1.29(10)	$E2$	$(37/2^+)$	$(33/2^+)$
13882(4)	1345(1)	1.2(4)	1.41(25)	$E2$	$(33/2^+)$	$(29/2^+)$

TABLE I. *(Continued.)*

E_x (keV)	E_γ (keV)	I_{rel} (%)	R_{30-83}	Multipolarity	J_i^π ($\hbar$)	J_f^π ($\hbar$)
12537(3)	3500(4)	0.7(2)		–	$(29/2^+)$	–
	5050(5)	0.5(2)	1.51(43)	$E2$	$(29/2^+)$	$25/2^+$
9037(2)	1408(2)	0.6(3)		–	–	$23/2^-$
ND8						
22903(7)	3128(4)	0.5(1)		$(E2)$[c]	$(47/2^-)$	$(43/2^-)$
19775(6)	2647(3)	0.8(2)		$(E2)$[c]	$(43/2^-)$	$(39/2^-)$
17128(5)	2309(3)	1.2(2)		$(E2)$[c]	$(39/2^-)$	$(35/2^-)$
14819(4)	1952(2)	0.8(3)		$(E2)$[c]	$(35/2^-)$	$(31/2^-)$
	4662(5)	0.8(3)		$(E2)$	$(35/2^-)$	$31/2^-$
12867(3)	3704(4)	0.1(1)		$(E2)$[a]	$(31/2^-)$	$27/2^-$
ND9						
22587(6)	3435(3)	0.5(2)		$(E2)$[c]	$(47/2^-)$	$43/2^-$
19152(5)	2711(3)	1.4(3)	1.81(42)	$E2$	$43/2^-$	$39/2^-$
16441(4)	2113(2)	2.5(5)	1.85(34)	$E2$	$39/2^-$	$35/2^-$
14328(3)	1660(2)	1.9(5)		$E2$[a]	$35/2^-$	$31/2^-$
	4170(4)	1.2(3)	1.42(22)	$E2$	$35/2^-$	$31/2^-$
12668(3)	3505(3)	2.2(3)	1.55(33)[b]	$E2$	$31/2^-$	$27/2^-$
ND10						
23902(6)	3258(3)	1.5(5)	1.49(35)	$E2$	$(49/2^-)$	$(45/2^-)$
20644(5)	2655(3)	3.9(5)	1.48(16)	$E2$	$(45/2^-)$	$(41/2^-)$
17989(4)	2248(2)	6.4(8)	1.52(17)	$E2$	$(41/2^-)$	$(37/2^-)$
15741(4)	1853(2)	6.5(7)	1.30(12)	$E2$	$(37/2^-)$	$(33/2^-)$
13888(3)	1549(2)	6.0(6)	1.41(12)	$E2$	$(33/2^-)$	$(29/2^-)$
	3731(3)	1.1(3)	1.32(19)	$E2/M1$[d]	$(33/2^-)$	$31/2^-$
SD3A						
24606(6)	2859(3)	0.5(2)		$(E2)$[c]	$(49/2^-)$	$(45/2^-)$
21747(5)	2475(3)	1.8(4)		$(E2)$[c]	$(45/2^-)$	$(41/2^-)$
19272(4)	2151(2)	2.5(5)		$(E2)$[c]	$(41/2^-)$	$(37/2^-)$
17121(4)	1020(1)	1.0(5)		$(E2/M1)$[c]	$(37/2^-)$	$(35/2^-)$
	1895(2)	2.0(4)		$(E2)$[c]	$(37/2^-)$	$(33/2^-)$
15226(4)	4559(5)	0.4(2)		$(E2)$[d]	$(33/2^-)$	$29/2^-$
SD3B						
26222(6)	3040(3)	0.7(2)	1.61(67)	$E2$	$(51/2^-)$	$(47/2^-)$
23182(6)	2649(3)	1.5(5)	1.53(34)	$E2$	$(47/2^-)$	$(43/2^-)$
20533(5)	2335(2)	2.0(4)	1.82(31)	$E2$	$(43/2^-)$	$(39/2^-)$
18198(4)	2097(2)	3.0(7)	1.67(29)	$E2$	$(39/2^-)$	$(35/2^-)$
16101(4)	875(1)	1.0(4)		$(E2/M1)$[c]	$(35/2^-)$	$(33/2^-)$
	4593(5)	0.7(3)		$(E2)$[d]	$(35/2^-)$	$31/2^-$
ND5						
15263(2)	1942(2)	2.4(6)		$E2$	$39/2^-$	$35/2^-$
14302(2)	980(1)	2.0(5)		$E2/M1$	$37/2^-$	$35/2^-$
	1831(2)	3.8(5)	1.30(17)	$E2$	$37/2^-$	$33/2^-$
13321(1)	850(1)	2.6(5)	0.95(8)[b]	$E2/M1$[c]	$35/2^-$	$33/2^-$
	1814(2)	4.6(6)	1.42(10)	$E2$	$35/2^-$	$31/2^-$
	3165(3)	1.1(3)		$E2$	$35/2^-$	$31/2^-$
12471(1)	963.6(6)	5.5(4)		$E2/M1$[c]	$33/2^-$	$31/2^-$
	1805(2)	4.8(5)	1.37(14)	$E2$[c]	$33/2^-$	$29/2^-$
11508(1)	840.7(6)	6.6(5)	0.95(8)[b]	$E2/M1$	$31/2^-$	$29/2^-$
	1446(2)	1.4(5)		$E2/M1$[a]	$31/2^-$	$29/2^-$
	1555(1)	7.2(8)	1.41(12)	$E2$	$31/2^-$	$27/2^-$
10667(1)	713.6(5)	11(1)	0.99(9)	$E2/M1$	$29/2^-$	$27/2^-$
	1362(1)	3.8(6)		$E2$[a]	$29/2^-$	$25/2^-$
9953(1)	583.3(6)	7.8(6)	1.00(10)	$E2/M1$	$27/2^-$	$25/2^-$
	647.6(5)	6.3(7)	0.93(11)	$E2/M1$	$27/2^-$	$25/2^-$

TABLE I. *(Continued.)*

E_x (keV)	E_γ (keV)	I_{rel} (%)	R_{30-83}	Multipolarity	J_i^π ($\hbar$)	J_f^π ($\hbar$)
	1175.9(4)	7.9(8)	1.60(20)	$E2$	$27/2^-$	$23/2^-$
9369(1)	592.0(4)	1.9(3)		$E2/M1$[a]	$25/2^-$	$23/2^-$
	2071(2)	1.7(6)	1.18(20)	$E1$[a]	$25/2^-$	$23/2^+$
9305(1)	528.0(6)	2.9(4)		$E2/M1$	$25/2^-$	$23/2^-$
	968(1)	1.0(2)		$E2$[a]	$25/2^-$	$21/2^-$
	1676(2)	2.8(7)	1.07(10)	$E2/M1$	$25/2^-$	$23/2^-$
	2006(2)	3.4(6)	0.94(11)	$E1$	$25/2^-$	$23/2^+$
8777(1)	439.9(4)	3.0(5)	0.98(11)	$E2/M1$	$23/2^-$	$21/2^-$
8337(1)	1039(1)	1.8(4)		$E1$[a]	$21/2^-$	$23/2^+$
	2246(2)	0.8(4)		$E1$[a]	$21/2^-$	$21/2^+$
	2785(2)	0.6(3)		$E1$[a]	$21/2^-$	$19/2^+$
	3142(3)	0.8(3)		$E2$[a]	$21/2^-$	$17/2^-$
	3691(3)	2.1(5)	1.27(36)	$E2$	$21/2^-$	$17/2^-$
Unlinked transitions						
10871(5)	4780(5)	1.1(3)	2.01(64)	($E2$)	$(25/2^+)$	$21/2^+$
11184(4)	3697(4)	1.2(3)	0.99(15)	$E2/M1$	$27/2^+$	$25/2^+$
11771(4)	4284(4)	0.8(2)	1.30(27)	$E2$	$(29/2^+)$	$25/2^+$
12763(4)	3600(4)	0.8(3)	2.08(68)	($E2$)	$(31/2^-)$	$27/2^-$
13212(3)	3055(3)	1.5(4)	0.68(15)	$\Delta I = 1$	33/2	$31/2^-$
14074(4)	3917(4)	2.3(4)	1.46(18)	$E2$	$35/2^-$	$31/2^-$
14116(4)	3959(4)	0.6(3)	0.85(30)	$\Delta I = 1$	33/2	$31/2^-$
14435(6)	5272(6)	0.3(2)	1.36(27)[b]	$E2$	$31/2^-$	$27/2^-$
14451(4)	4294(4)	0.8(3)	1.56(23)	$E2$	$35/2^-$	$31/2^-$
14771(5)	4614(5)	0.7(2)		–	–	$31/2^-$
15022(5)	4865(5)	0.7(3)	0.91(26)	$E2/M1$	$33/2^-$	$31/2^-$
15295(5)	5138(5)	0.6(2)		–	–	$31/2^-$

[a]Defined by parallel transitions or connecting cascades.
[b]Doublet structure.
[c]Inferred by rotational behavior.
[d]Supported by yrast arguments.

and, in addition, the low-spin part of the level scheme into which the transitions enter is dominated by several transitions with very similar energies such as the 1534 and 1538, the 1677 and 1676, and the 1396 and 1403 keV transitions. This means that the spin-parity assignment of the structure is not very easily determined. The strongest linking transition is the 5278 keV γ ray with an intensity ratio indicating an $E2$ character. This assignment is further supported via the 5314 keV transition, which also seems to be an $E2$ connection. The maximum observed spin of the structure is then $I^\pi = 57/2^+$ at an excitation energy of $E_x = 29\,171$ keV.

Coincidences with the 5278 keV, $25/2^+ \rightarrow 21/2^+$ decay-out transition are illustrated in Fig. 2. The rotational band is here very clearly indicated together with two γ-ray transitions originating from the low-spin part of the level scheme.

B. Structure SD2

Structure SD2 consists of three SD bands connected via dipole transitions at lower excitation energies. The structure is only connected to the low-spin level scheme via one tentative transition at 3109 keV, resulting in a tentative spin-parity assignment. Structures SD2A and SD2C have a tentative maximum spin-parity assignment of $I^\pi = (53/2^-)$ at an excitation energy of $E_x = 25\,451$ and $E_x = 25\,282$ keV, respectively. Correspondingly, SD2B has $I^\pi = (55/2^-)$ at $E_x = 27086$ keV. The relative intensity of each of the three bands is around 2% of the 124 keV ground-state transition.

The coincidences in band SD2A can be seen in the top panel of Fig. 3. The spectrum is in coincidence with the 2380 keV, $(45/2^-) \rightarrow (41/2^-)$ transition. The coincident transitions within the band are labeled.

The coincidences in band SD2B can be seen in the middle panel of Fig. 3. The spectrum is gated on the 2857 $\rightarrow$ 2528 $\rightarrow$ 2241 keV cascade. Transitions in the structure are marked.

The coincidences in band SD2C can be seen in the bottom panel of Fig. 3. The spectrum is gated on the 2586 keV, $(49/2^-) \rightarrow (45/2^-)$ transition. The coincidences with the transitions in the structure are indicated in the spectrum.

C. Structure ND7

Structure ND7 is connected to the low-spin level scheme via two linking transitions: one direct at 5050 keV, and one via an intermediate state, the 3500–1408 keV cascade. The spin-parity assignment of the structure is based on the R_{30-83}

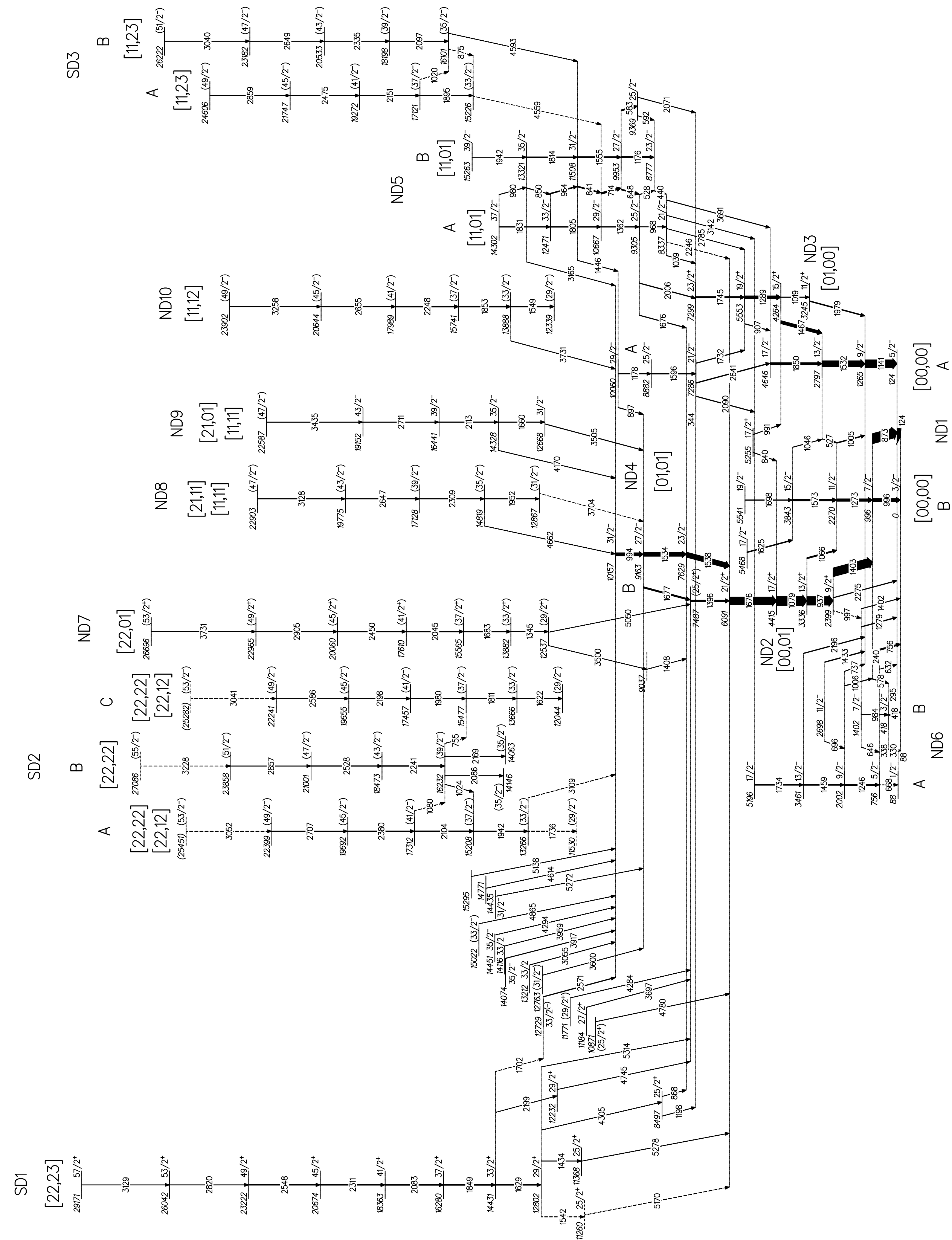

FIG. 1. Excitation scheme of ^{61}Zn from the present work. The widths of the arrows correspond to the relative intensities of the transitions. Tentative transitions and levels are dashed. Each structure is given a short-hand notation, and the standard CNS labeling of each configuration is also indicated.

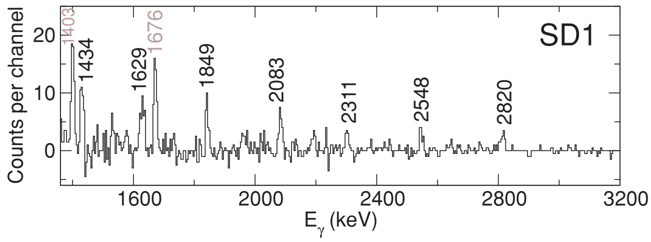

FIG. 2. (Color online) Spectrum in coincidence with the 5278 keV, $25/2^+ \rightarrow 21/2^+$ decay-out transition in structure SD1. This spectrum is TE gated, and all peaks marked with an energy label are placed into the decay scheme of Fig. 1. If the label is indicated in black, the γ ray belongs to the SD structure, gray indicates that they originate from the low-spin part of the level scheme. The spectrum is binned 4 keV/channel.

value of the directly linking transition which indicates $E2$ character. However, the large uncertainty of this value makes the assignment tentative. At the highest energy level, $E_x = 26\,696$ keV, the structure reaches $I^\pi = (53/2^+)$. The relative intensity of the structure is around 4% of the 124 keV ground-state transition.

Figure 4 illustrates coincidences with the 2905 keV, $(49/2^+) \rightarrow (45/2^+)$ transition. In addition to the transitions from the structure itself, some transitions from the low-spin part of the level scheme are indicated as well as the connecting transition at 3500 keV.

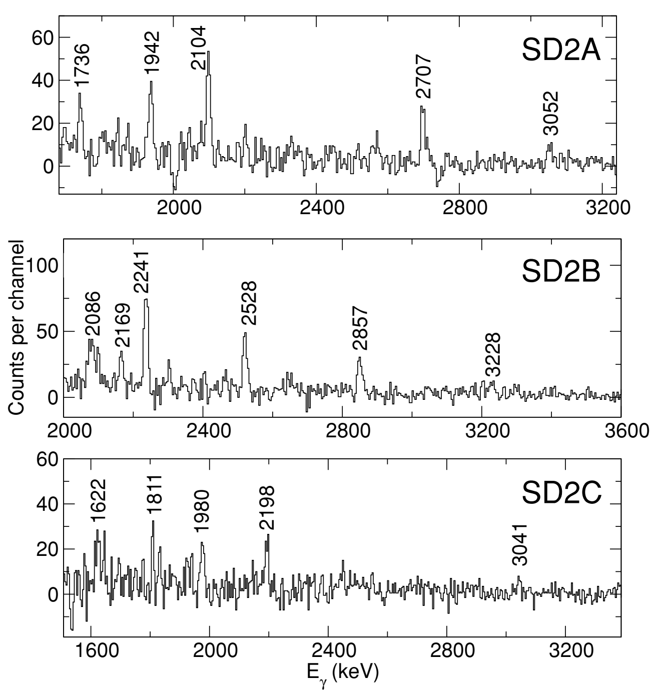

FIG. 3. Same as Fig. 2, but in coincidence with (top) the 2380 keV, $(45/2^-) \rightarrow (41/2^-)$ transition in structure SD2A; (middle) any of the transitions in the $2857 \rightarrow 2528 \rightarrow 2241$ keV cascade in structure SD2B; (bottom) the 2586 keV, $(49/2^-) \rightarrow (45/2^-)$ transition in structure SD2C. Each spectrum is TE gated and binned 4 keV/channel.

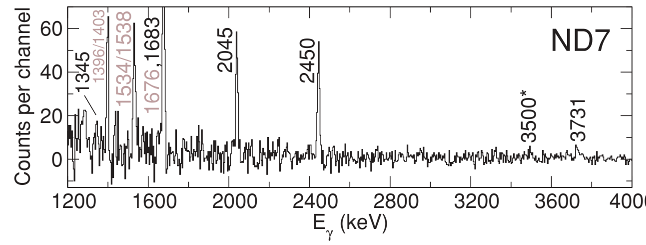

FIG. 4. (Color online) Same as Fig. 2, but in coincidence with the 2905 keV, $(49/2^+) \rightarrow (45/2^+)$ transition in structure ND7. Transitions marked with a star indicate connecting transitions between structure ND7 and the rest of the level scheme. The spectrum is TE gated and binned 4 keV/channel.

D. Structure ND8

Structure ND8 is the weakest structure in this study, with a relative intensity of around 1% of the 124 keV ground-state transition. The low intensity implies that intensity ratios are impossible to determine. Spin and parity are instead preliminarily assigned using yrast arguments. At the highest energy level, $E_x = 22\,903$ keV; the structure thus reaches $I^\pi = (47/2^-)$. Figure 5 illustrates a spectrum containing coincidences with the 4662 keV linking transition, which has a relative intensity of only 0.8 units. Two of the transitions in structure ND8 can clearly be seen in the spectrum.

E. Structure ND9

Structure ND9 has two γ-ray transitions, at 4170 and 3505 keV, connecting the structure to the low-spin level scheme. Both transitions indicate $E2$ character, but the latter is energetically close to the $(29/2^+) \rightarrow (25/2^+)$ transition decaying out from structure ND7 resulting in a less reliable R_{30-83} value. Based on the character of the two decay-out transitions, the structure has been assigned both spin and parity. At the most energetic level in the structure, $E_x = 22\,587$ keV, $I^\pi = (47/2^-)$ is reached. The relative intensity of the structure is some 2% of the 124 keV ground-state transition. In Fig. 6, coincidences with the 2711 keV, $43/2^- \rightarrow 39/2^-$ transition are shown. The transitions in the structure as well as the linking transitions can be seen in this spectrum. Note that this transition is energetically close to the 2707 keV transition in structure SD2A, resulting in some peaks from this structure appearing in Fig. 6 as well.

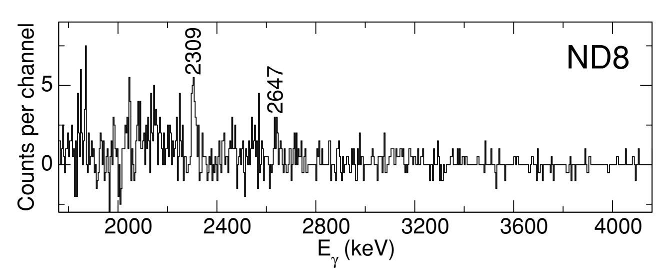

FIG. 5. Same as Fig. 2, but in coincidence with the 4662 keV connecting transition in structure ND8. The spectrum is TE gated and binned 4 keV/channel.

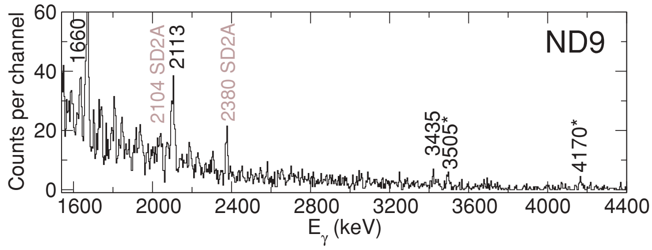

FIG. 6. (Color online) Same as Fig. 2, but in coincidence with the 2711 keV, $43/2^- \rightarrow 39/2^-$ transition in structure ND9. Note the coincidences with the 2707 keV transition in structure SD2A. Transitions marked with a star indicate connecting transitions between structure ND9 and the rest of the level scheme. The spectrum is TE gated and binned 4 keV/channel.

F. Structure ND10

Structure ND10 has a tentative spin-parity assignment in the current analysis. The assignment is based on the 3731 keV transition connecting the band with the $31/2^-$ energy level at 10157 keV in the low-spin level scheme. However, for the transition, an intensity ratio of $R_{30-83} = 1.32(19)$ has been obtained. This ratio can be interpreted both as an $E2$ and as a mixed $E2/M1$ transition.

Considering the intensities of the γ-ray transitions in this structure compared to structure SD1 a mixed $E2/M1$ character is suggested. This argument is based on, for example, the comparison between the decay out from the 20674 keV, $45/2^+$ state in SD1 which has a relative intensity of 4.3(5). Assuming mixed $E2/M1$ character of the decay out in ND10 makes the energy level at 20 644 keV a $45/2^-$ state. The decay-out transition has a relative intensity of 3.9(5). The agreement between relative intensities is what is to be expected for states of similar energies and spins. If instead an $E2$ character of the decay-out transition were assumed, then structure ND10 would be yrast, and hence larger relative intensities would be expected. The spin assignment is discussed further in relation to the cranked Nilsson-Strutinsky predictions. If interpreting the 3731 keV transition as being of mixed $E2/M1$ character, structure ND10 reaches a tentative spin of $I^\pi = (49/2^-)$ at an excitation energy of $E_x = 23902$ keV.

Figure 7 illustrates the coincidences with either the 2655 or the 2248 keV γ-ray transitions. All the transitions from structure ND10 are indicated in the spectrum. A few transitions

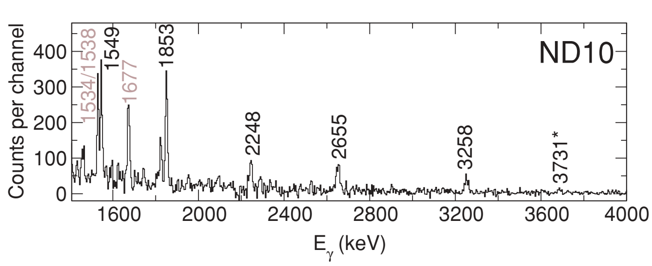

FIG. 7. (Color online) Same as Fig. 2, but in coincidence with either of the transitions in the 2655–2248 keV cascade in structure ND10. Transitions marked with a star indicate connecting transitions between structure ND10 and the rest of the level scheme. The spectrum is TE gated and binned 4 keV/channel.

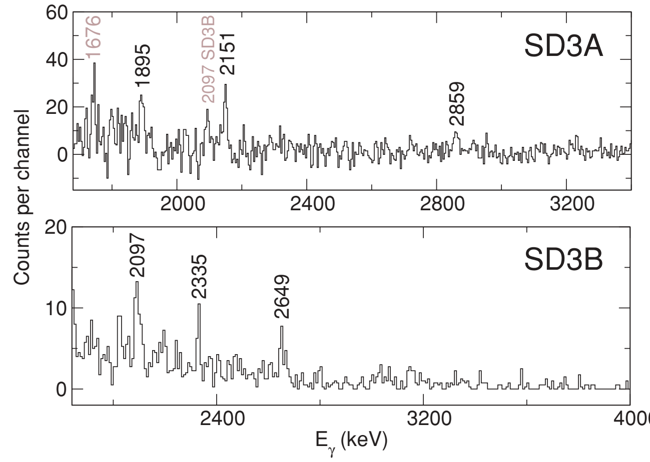

FIG. 8. (Color online) Same as Fig. 2, but in coincidence with (top) the 2475 keV, $(45/2^-) \rightarrow (41/2^-)$ transition in structure SD3A; (bottom) the 4593 keV linking transition in structure SD3B. Both spectra are TE gated and binned 4 keV/channel (8 keV/channel) for the top (bottom) panel.

originating from the low-spin part of the level scheme are also included.

G. Structure SD3

Structure SD3 consists of two bands that are found to be signature partners. The structure is connected to ND5 via one tentative, 4559 keV, and one firmly determined, 4593 keV, connecting transition. Neither of these are intense enough to provide an R_{30-83} value to determine the spin and parity of the structure. The two transitions are suggested as $E2$ transitions based on yrast arguments resulting in a maximum tentative spin of SD3A (SD3B) at $I^\pi = 49/2^-$ ($I^\pi = 51/2^-$) at an excitation energy of $E_x = 24\,606$ keV ($E_x = 26\,222$ keV).

The top panel of Fig. 8 shows a spectrum with coincidences with the 2475 keV transition in SD3A. The spectrum illustrates the transitions in the band as well as a coincidence with a 2097 keV transition most likely to originate from structure SD3B. The $\Delta I = 1$ transitions between the two bands are, however, weak and have not been clearly identified.

The bottom panel of Fig. 8 shows a spectrum with coincidences with the 4593 keV linking transition between SD3A and the low-spin level scheme. In spite of the very low intensity, 0.7% of the ground-state transition, the spectrum clearly indicates the three lowest γ-ray transitions from the structure.

H. Structure ND5

Structure ND5 consists of two signature partners which are built from quadrupole transitions and connected via intense dipole transitions between them. The quadrupole (dipole) transitions have an overall yield of some 5% (10%) of the ground-state transition. The maximum spin is $I^\pi = 37/2^-$ at $E_x = 14\,302$ keV for structure ND5A and $I^\pi = 39/2^-$ at $E_x = 15\,263$ keV for structure ND5B. The structure is connected to the rest of the level scheme with ten γ-ray transitions. For four of these, the intensity ratio is determined.

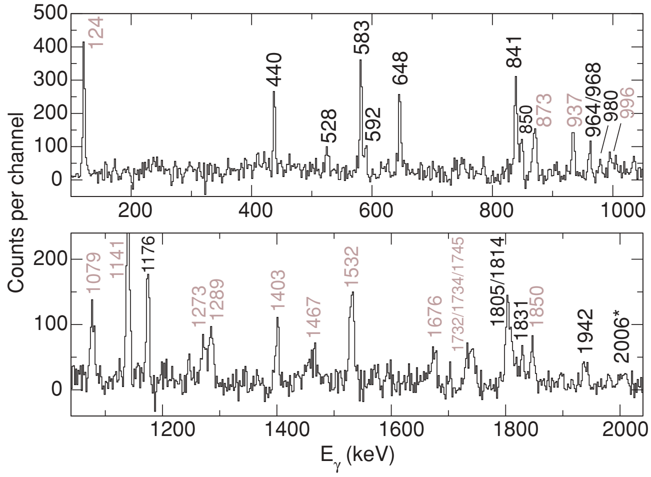

FIG. 9. (Color online) Same as Fig. 2, but in coincidence with the 714 keV, $29/2^- \rightarrow 27/2^-$ transition in structure ND5. Transitions marked with a star indicate connecting transitions between structure ND5 and the rest of the level scheme. The spectrum is TE gated and binned 2 keV/channel.

These transitions provide a firm spin-parity assignment of the structure.

Figure 9 illustrates coincidences with the intense $29/2^- \rightarrow 27/2^-$ 714 keV transition placed in the middle of the structure. Here, γ-ray transitions originating from both ND5A and ND5B are seen as well as the dipole transitions between them.

I. Unlinked transitions

In the present analysis, more than ten highly energetic γ-ray transitions were found connected to the low-spin part of the level scheme but not linked to any of the observed high-spin structures. The transitions can be found on the left-hand side in the level scheme in Fig. 1. A spectrum indicating these transitions as well as some of the transitions linking or originating from structures SD1–SD3 and ND7–ND10 is seen in Fig. 10. The spectrum is gated on γ-ray transitions with high intensities originating from the low-spin part of the level scheme, and most of the unlinked transitions are indicated in spite of their low intensities of less than 1% of the 124 keV ground-state transition.

IV. CNS CALCULATIONS AND CLASSIFICATION OF STRUCTURES

The structures described in Sec. III are discussed here in relation to the predictions using configuration-dependent cranked Nilsson-Strutinsky (CNS) calculations. The CNS calculations [7,25] are based on the cranking model [26,27], in which the single-particle eigenvalues are calculated using the Nilsson Hamiltonian [28,29]:

$$h = -\frac{\hbar^2}{2M}\Delta + \frac{1}{2}M\left(\omega_z^2 z^2 + \omega_x^2 x^2 + \omega_y^2 y^2\right) - 2\kappa\hbar\omega_0 \vec{l}\cdot\vec{s} - \mu\kappa\hbar\omega_0(\vec{l}^2 - \langle\vec{l}^2\rangle_{\mathcal{N}}). \quad (1)$$

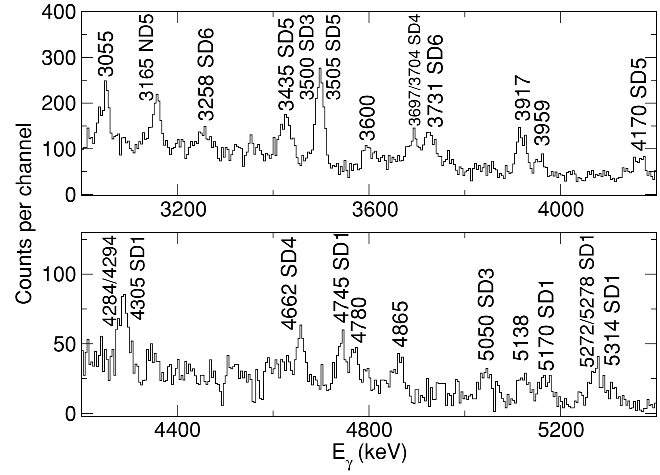

FIG. 10. Same as Fig. 2, but in coincidence with either of the transitions in the $1676 \rightarrow 1079 \rightarrow 937 \rightarrow 1403$ keV cascade in the low-spin part of the level scheme. The focus is on high-energy γ-ray transitions. In relevant cases, the structure to which the transition is linked is indicated. The spectrum is TE gated and binned 4 keV/channel.

Deformations are included by allowing the three oscillator frequencies to vary. It is common to express the frequencies in quadrupole deformation parameters (ϵ_2, γ) and then add a term that describes the hexadecapole deformations (ϵ_4). The standard values of the Nilsson parameters κ and μ are used. These are of empirical origin and taken from Ref. [25]. The values differ slightly between neutrons and protons and vary for the different shells, i.e., for each main oscillator quantum number $\mathcal{N}$.

In the calculations, configurations are fixed, and the total energy is then minimized in terms of deformation using the parameters above. The pairing effects are neglected in the model, as the calculations are aimed at describing structures at high angular momenta. In the mass $A \sim 60$ region, the effects of pairing become important at spins below some $10\hbar$.

Standard cranked Nilsson-Strutinsky labeling of each rotational band will be used in the following. This short-hand notation is based on the number of particles in different j shells for each configuration. The j shells are pure only if the shape is spherical. Thus, in general the labeling refers to the dominating shell only, while the wave functions also contain components from other $\mathcal{N}$ and j shells. Relative to a closed ^{56}Ni core, a configuration can be written as

$$\pi(1f_{7/2})^{-p_1} \otimes \pi(1g_{9/2})^{p_2} \otimes \pi(fp)^{p_3} \otimes, \\ \nu(1f_{7/2})^{-n_1} \otimes \nu(1g_{9/2})^{n_2} \otimes \nu(fp)^{n_3}, \quad (2)$$

which provides a possibility of giving the short-hand notation $[p_1 p_2, n_1 n_2]$. Here, p_1 and n_1 denote the number of holes in the orbitals of high-j $1f_{7/2}$ character, and similarly p_2 and n_2 denote the number of particles in the high-j $1g_{9/2}$ subshell. The remaining orbitals between the $N = Z = 28$ and the $N = Z = 50$ shell gaps are referred to as fp and are all considered to be of low-j character. These are the $1f_{5/2}$, $2p_{3/2}$, and the $2p_{1/2}$ subshells. The parameters p_3 and n_3 denote the number of particles in these subshells.

In Figs. 11–13, the results of the experimental analysis are compared with the predictions using the CNS model via three panels. Each of the top panels illustrates the structures with their experimentally observed energies and spin-parity assignments. The y axis denotes the energy with the rotating liquid drop (rld) energy [30] subtracted. The x axis represents the spin of the level. The middle panels illustrate the same but for the chosen predicted configurations. In the bottom panels, the energy differences between the predictions and the observations are plotted.

The calculations in the current analysis are performed with the methods introduced in Ref. [30], so that not only the relative energies between the bands but also the absolute scale can be compared. Low-spin states are generally predicted too high in energy because of the neglected pairing interaction. The high-spin states on the other hand should agree with the experimental results within a typical uncertainty of ± 1 MeV. Ideally the observed transition energies will be predicted correctly by the calculations for each transition within a band. If this is the case, the band in the bottom panel will have a constant energy difference for all states of a given configuration or structure, i.e., it will be horizontal.

Each band in the three panels is indicated according to its spin and parity assignment. Positive (negative) signature is drawn with filled (open) symbols. Solid (dashed) lines represent positive (negative) parity.

An overview of the results from the matching between the experimental structures and predicted configurations is found in Table II. Different proton (rows) and neutron (columns) configurations are combined; and for each combination, the maximum spin I_{max}, defined from the pure j-shell configuration, is given. The table also indicates results from previously published data in the mass $A \sim 60$ region for comparison.

A. Low-spin structures

The predictions for the low-spin structures in ^{61}Zn are shown in Fig. 11. In the top panel, the notation for each band corresponds to the ones given in Fig. 1.

As mentioned earlier, the omitted pairing force will result in less reliable energy predictions for low-spin structures. The effect of this can be seen in this figure. As spin increases, the bands in the lowest panel tend to move toward a smaller absolute energy difference. For structures ND1 and ND2 the bands are matched with configurations [00,00] and [00,01], respectively. It is questionable whether the more excited ND3 band should be assigned to a pure CNS configuration, but one can note that it is reasonably well described by a [01,00] configuration, which is also the $(\pi, \alpha) = (+, -1/2)$ configuration calculated to be lowest in energy.

The general trend at low spins indicates that the likelihood of exciting a particle from the upper fp shell into the $1g_{9/2}$ orbital is larger than that of creating a hole in the $1f_{7/2}$ shell for the low-spin structures. This trend is true also for other nuclei in this mass region, see Table II.

At higher spins, structures ND4 and ND5 are found. The energy differences in the lowest panel of Fig. 11 are smaller for these structures and within the expected ± 1 MeV. Structure ND4 only involves two energy states for each signature partner, connected via the 1178 keV (ND4A) and the 994 keV (ND4B) γ-ray transitions. In spite of the few data points, ND4 makes an excellent match with the predicted [01,01] configuration. It is typical for configurations dominated by high-j particles like this to only be observed close to termination. This is understood from the fact that they are predicted to rapidly become non-yrast as the spin values decrease.

Structure ND5 is the only structure found in ^{61}Zn that is dominated by the strong dipole transitions between the two

TABLE II. Experimentally observed structures are shown to illustrate their configuration assignments. Horizontal rows illustrate the proton configurations and the vertical columns give neutron configurations. For each combined neutron-proton configuration, the maximum spin is indicated as well as the experimental bands found for ^{61}Zn and/or other mass $A \sim 60$ nuclei.

Config. ν		00]	01]	11]	02]	12]	22]	23]
π	I_{max}	11/2	17/2	27/2	21/2	31/2	39/2	41/2
[00		ND1	ND2					
	8/2	19/2[a,c,d]	25/2[a,c,d]	35/2[a]	29/2	39/2	47/2	49/2
[01		ND3	ND4					
	14/2	25/2[a]	31/2[a,c,d]	41/2	35/2[c]	45/2	53/2	55/2
[10								
	18/2	29/2[a]	35/2[a,d,e]	45/2[a]	39/2[e]	49/2	57/2	59/2
[11			ND5	(ND8, ND9)		ND10		SD3
	24/2	35/2[a]	41/2[c,d,e]	51/2[a]	45/2[c,d]	55/2	63/2	65/2
[21			(ND9)	(ND8)				
	32/2	43/2	49/2[a,e]	59/2[a,b,d]	53/2[d]	63/2[d]	71/2[a,b,d]	73/2
[22			ND7			SD2	SD2	SD1
	36/2	47/2	53/2[c]	63/2[a,b]	57/2	67/2	75/2[a,b]	77/2

[a]Structures with this configuration were observed in ^{59}Cu [1].
[b]Structures with this configuration were observed in ^{58}Ni [3].
[c]Structures with this configuration were observed in ^{62}Zn [6].
[d]Structures with this configuration were observed in ^{61}Cu [14].
[e]Structures with this configuration were observed in ^{60}Ni [31].

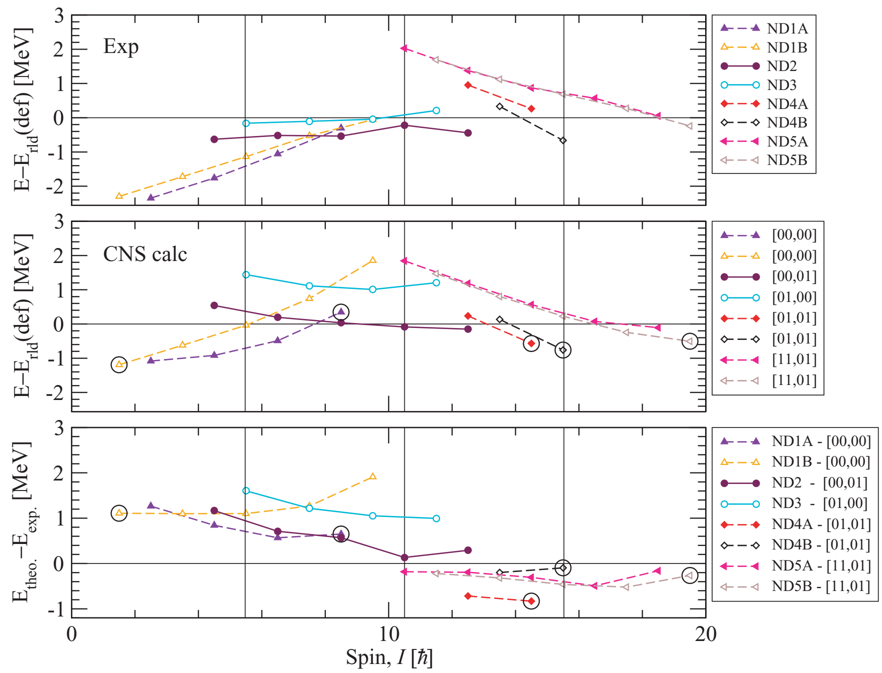

FIG. 11. (Color online) Comparison between experimentally observed structures and CNS predictions in the low-spin part of the level scheme in ^{61}Zn. The top panel illustrates the experimental results where the bands are labeled according to Fig. 1. The middle panel shows the chosen predicted bands. The bottom panel plots the energy difference between the prediction and observation. Note the clear correlation between the maximum spin values and the number of particles excited from the $1f_{7/2}$ and into the $1g_{9/2}$ orbital. Encircled points correspond to states with $\gamma = 60^{\circ}$. For details see text.

signature partners. Previous studies [14,31] show that these structures are not uncommon in this mass region. ND5 is matched with a [11,01] configuration, and the agreement is very good. The small observed signature splitting indicates an odd $1f_{7/2}$ hole, agreeing with the matched configuration. Nearly horizontal lines result at low values of $E_{\text{theo.}} - E_{\text{exp.}}$ in the bottom panel of Fig. 11.

Structure ND6 has not been assigned a CNS configuration in the present analysis. The low spins and observed intensities suggest that this structure should be formed via an excitation of the odd neutron from the [00,00] configuration of structure ND1. The energy of such an excited band is not a straightforward prediction using the CNS calculations. Since the low-spin structures are less reliable in the predictions—because of the neglected pairing force—the band is not included in Fig. 11.

B. High-spin structures

The predictions for the high-spin structures in ^{61}Zn are shown in Figs. 12 and 13. In the top panel on both figures, the notation of each band corresponds to the ones given in Fig. 1; structure SD1 is included in both figures as a point

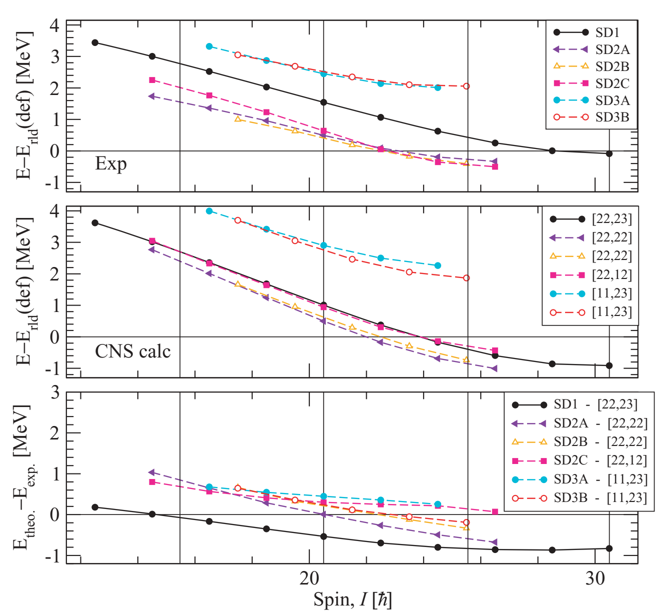

FIG. 12. (Color online) Same as Fig. 11, but for the high-spin structures assigned to configurations predicted with $I_{\max} > 30$.

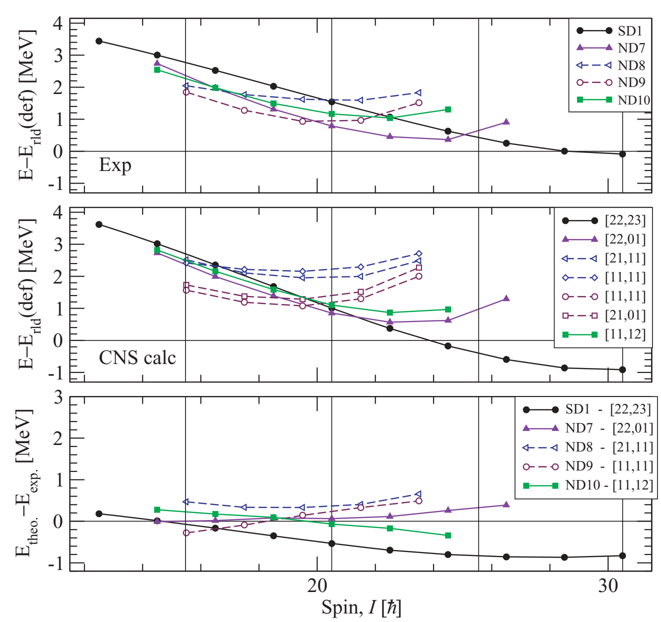

FIG. 13. (Color online) Same as Fig. 11, but for the high-spin structures predicted with $I_{\max} < 30$. Band SD1 is included for reference.

of reference. The separation of the bands into the two figures is based on their general behavior as a function of spin. In Fig. 12, the bands which are favored in energy at high spins are illustrated. If denoting the number of excitations from the $1f_{7/2}$ subshell by $q_1 = p_1 + n_1$ and the number of excitations into the $1g_{9/2}$ subshell by $q_2 = p_2 + n_2$, the total number of excitations can be denoted $q = q_1 + q_2$. These bands have a larger number of excitations, q, than the unfavored ones, i.e., the bands plotted in Fig. 13.

With the spin assignments from the present analysis, structure SD1 corresponds to a [22,23] configuration, as was suggested in Ref. [5]. The resulting band in the bottom panel of Fig. 12 shows a good agreement with the experimental data. Even the effect of pairing can be seen at lower spins.

The three bands in structure SD2 are matched with a [22,22] configuration for SD2B with either band A or C being its signature partner. Both bands end at approximately the same energy, making a distinction between them impossible. The band that is not a signature partner to SD2B has been assigned a [22,12] configuration. For the bottom panel of Fig. 12, bands A and B are chosen to be signature partners. The bands assigned to SD2 ([22,22] and [22,12]) are calculated close in energy to the [22,23] configuration (SD1), as previously discussed in Ref. [5]. The conclusions made in Ref. [5] are valid and confirmed in the current analysis, especially via the observation of the [22,22] bands.

The two bands in SD3 are interpreted as signature partners and agree well with a [11,23] configuration. The small observed signature splitting indicates an odd $1f_{7/2}$ hole, which agrees well with the matched configuration. The predicted signature splitting is, however, a little larger than what is experimentally observed. Note that the experimental dipole transitions between the bands are tentative, as is the linking transition between SD3A and ND5. An alternative option for a matching configuration with an odd $1f_{7/2}$ hole that would form high enough spins is the [12,22] configuration. However, this match seems less likely, as it is predicted to be some 0.5 MeV higher in energy. In addition, in Ref. [14] it was suggested that the standard Nilsson parameters κ and μ should be modified to improve the agreement between predictions and the observed structures in this mass region. It should be noted that by increasing κ by 10% in the $\mathcal{N} = 3$ shell, the predicted signature splitting between the [11,23] bands decreases, improving the agreement between the experimental observation and the predictions.

Structure ND7 yields good agreement with the [22,01] configuration. On the other hand, for structure ND8, two possible configurations have to be considered: either [11,11] or [21,11]. Both end up at similar energies. The latter is slightly lower in energy and hence used for the plot in the bottom panel. Structure ND9 also can be matched with two possible configurations that are very similar in energy: [11,11] and [21,01]. The former is here used in the bottom panel of Fig. 13, but their energy separation is too small to rule out either configuration. It should, however, be noted that a degenerate signature partner would be expected for [11,11] but not for [21,01]. This fact rather supports the latter assignment.

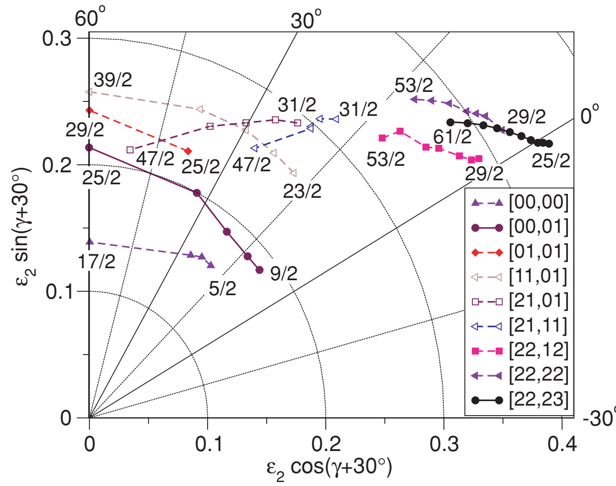

FIG. 14. (Color online) Calculated shape evolutions for a selection of the observed bands. The trajectories are drawn only for the observed states with $\Delta I = 2$.

Structure ND10 is in excellent agreement with configuration [11,12]. This agreement, however, is based on the assumption that the 3731 keV linking transition is of mixed $E2/M1$ character. As previously mentioned, the multipolarity can be questioned especially in relation to the experimentally observed high intensity of this structure. However, there would be no predicted bands to readily match this structure if a pure $E2$ multipolarity were to be assigned. The increased spin would position the band around 1 MeV lower in energy, i.e., at even lower energies than the SD2 structure described above. As this seems unlikely, the tentative spin assignment found in Fig. 1 is kept.

C. Deformations

The calculated shape trajectories of a selection of the experimentally observed bands are shown in Fig. 14. As a general trend, the shapes change gradually from prolate ($\gamma = 0^\circ$) to oblate ($\gamma = 60^\circ$) where termination occurs. The earlier observed trend [1,14] of deformation increasing with q, the sum of the number of holes in the $1f_{7/2}$ and particles in the $1g_{9/2}$ subshell, is illustrated in this plot. The illustrated bands range from $q = 0$ to $q = 9$, and the ϵ_2 deformations—the distance from the origin—increase with increasing q.

V. SUMMARY

The experimental level scheme of ^{61}Zn has been greatly extended in the current analysis to include some 180 γ-ray transitions connecting some 120 energy levels. Almost every level has been assigned firm or tentative spin and parity. The level scheme ranges up to spin $I = 57/2$ at an excitation energy of more than 29 MeV, and a total of seven high-spin structures dominated by quadrupole transitions have been identified. These and five low-lying structures have been explored using cranked Nilsson-Strutinsky calculations. Each band has been matched with a possible configuration, revealing, in general, good agreement with the experimental data.

The previously published SD band in ^{61}Zn from Ref. [5] has been explored in detail, resulting in a modified decay-out pattern. The final conclusion is a confirmation of the tentative spin assignments from Ref. [5] and that the discussion around this structure is valid.

According to Ref. [14], the explored structures can be used to adjust the standard Nilsson parameters. First results show that the modifications suggested in Ref. [14] would improve the agreement with the experimental data presented here.

ACKNOWLEDGMENTS

We thank the accelerator crew and the GAMMASPHERE support staff at Argonne National Laboratory for their supreme efforts. Our thanks also go to D. P. Balamuth, J. Eberth, A. Galindo-Uribarri, P. A. Hausladen, and Th. Steinhardt for their help and support during the experiments. This work is supported in part by the Swedish Research Council and the US Department of Energy, Office of Nuclear Physics, under Contract Nos. DE-FG05-88ER-40406 (WU) and DE-AC02-06CH11357 (ANL).

[1] C. Andreoiu *et al.*, Eur. Phys. J. A **14**, 317 (2002).
[2] E. K. Johansson *et al.*, Phys. Rev. C **77**, 064316 (2008).
[3] D. Rudolph *et al.*, Phys. Rev. Lett. **96**, 092501 (2006).
[4] C. E. Svensson *et al.*, Phys. Rev. Lett. **82**, 3400 (1999).
[5] C.-H. Yu *et al.*, Phys. Rev. C **60**, 031305(R) (1999).
[6] C. E. Svensson *et al.*, Phys. Rev. Lett. **80**, 2558 (1998).
[7] A. V. Afanasjev, D. B. Fossan, G. J. Lane, and I. Ragnarsson, Phys. Rep. **322**, 1 (1999).
[8] R. B. Schubank, J. A. Cameron, and V. P. Janzen, Phys. Rev. C **40**, 2310 (1989).
[9] S. M. Vincent *et al.*, Phys. Rev. C **60**, 064308 (1999).
[10] M. R. Bhat, Nucl. Data Sheets **88**, 417 (1999).
[11] L.-L. Andersson *et al.*, Eur. Phys. J. A **30**, 381 (2006).
[12] O. Izotova *et al.*, Phys. Rev. C **69**, 037303 (2004).
[13] I.-Y. Lee, Nucl. Phys. **A520**, 641c (1990).
[14] L.-L. Andersson *et al.*, Eur. Phys. J. A **36**, 251 (2008).
[15] D. Rudolph *et al.*, Eur. Phys. J. A **4**, 115 (1999).
[16] D. G. Sarantites *et al.*, Nucl. Instrum. Methods Phys. Res. A **530**, 473 (2004).
[17] D. G. Sarantites *et al.*, Nucl. Instrum. Methods Phys. Res. A **381**, 418 (1996).
[18] D. Rudolph *et al.*, Eur. Phys. J. A **14**, 137 (2002).
[19] C. J. Chiara *et al.*, Nucl. Instrum. Methods Phys. Res. A **523**, 374 (2004).
[20] D. Seweryniak, J. Nyberg, C. Fahlander, and A. Johnsson, Nucl. Instrum. Methods Phys. Res. A **340**, 353 (1994).
[21] D. A. Torres, Ph.D. thesis, Universidad Nacional de Colombia (2007).
[22] C. E. Svensson *et al.*, Nucl. Instrum. Methods Phys. Res. A **396**, 228 (1997).
[23] D. C. Radford, Nucl. Instrum. Methods Phys. Res. A **361**, 297 (1995).
[24] J. Theuerkauf, S. Esser, S. Krink, M. Luig, N. Nicolay, O. Stuch, and H. Wolters, Program TV, University of Cologne (unpublished).
[25] T. Bengtsson and I. Ragnarsson, Nucl. Phys. **A436**, 14 (1985).
[26] D. R. Inglis, Phys. Rev. **96**, 1059 (1954).
[27] D. R. Inglis, Phys. Rev. **103**, 1786 (1956).
[28] S. G. Nilsson *et al.*, Nucl. Phys. **A131**, 1 (1969).
[29] S. G. Nilsson and I. Ragnarsson, *Shapes and Shells in Nuclear Structure* (Cambridge University, Cambridge, England, 1995).
[30] B. G. Carlsson and I. Ragnarsson, Phys. Rev. C **74**, 011302(R) (2006).
[31] D. A. Torres *et al.*, Phys. Rev. C **78**, 054318 (2008).